Proceedings of the 2002 IEEE
International Conference on Robotics & Automation
Washington, DC • May 2002

# Contact Point Identification in Multi-Fingered Grasps Exploiting Kinematic Constraints

S. Haidacher and G. Hirzinger

German Aerospace Center - DLR
Institute for Robotics and Mechatronics
82230 Wessling, Germany
E-mail: Steffen.Haidacher@dlr.de

**Abstract** — *Most of the algorithms used in grasp planning, force optimization and control of multi-fingered hands need information about the points of contact with a grasped object as well as the normal of the surface in the contact point. With no image processing, this information is gained from tactile sensor arrays, multidimensional force/torque sensors or a priori knowledge. This paper presents a method for those cases, when no good quality sensors are present or measurements are to be improved by sensor fusion. An algorithm is developed to determine the contact points and inherently the surface normal from only joint angle sensors and a geometric description of the fingertip in the 3D case. This is done by observing the constrained motion of fingers securely grasping an object.*

## 1. Introduction

Grasping with dextrous hands has been a topic of research for the last two decades and several dextrous robotic maipulators have been constructed in the meantime [6, 7, 1], c.f. figure 1. Hereby, research is performed mostly in two areas, first the exploration and modelling of an unknown object and second grasping and manipulation of a known object. In the first area, strategies have been developed to explore the geometry of an object [16, 10], to model an object from measured data [8, 9] or to exploit and interprete information obtained from a tactile sensor [23, 2]. On the other hand, methods to synthesize appropriate grasps have been developed adressing the problem in quite different ways [12, 13, 4]. In order to control the position of objects, several control schemes have been introduced [19]. To determine the optimal force to apply to the object, several algorithms have been presented [5]. Either of these algorithms, however, needs information about the contact between the object and the fingers of the hand. Of particular interest is hereby the exact position and the normal direction of the object's surface to cope with Coulomb friction constraints for maintaining stable contact. Considering contact models like rolling contacts, this information may vary over time. Particularly with respect to the latter, a full object exploration is neither feasible nor necessary since only local *exteroceptive* [8] information is required. In literature, there exist two different methods to gain this information and eventually information about object pose and motion, on the one hand through an *array-type* tactile measurement [2, 14, 18] or on the other hand through *intrinsic* measurement of forces and torques and reconstruction of the contact point [19, 3, 24]. Only little research has been done gaining information from kinematic constraints through the contact of multiple fingers with the object. In general, this idea relies on motion between the individual fingers and the object, which can be achieved by compliance control of the fingers and moving the object through another finger or interaction with the environment. This methodology can be used when neither *intrinsic* nor *array-type* sensors are present as in simple grippers or to gain additional contact information for a higher precision by sensor fusion. It can also be applied, when the contact between finger and object admits some torque tangential to the contact surface as in grasps with flat, soft, human-like fingers. Previous work [15] detects the point of contact from intersection of two different positions in space of the same link. This is extended with a position correction term and a spherical geometry in the finger tip by [11]. [20] determines the contact location from joint position and torque measurements while disturbing the grasp infinitesimally.

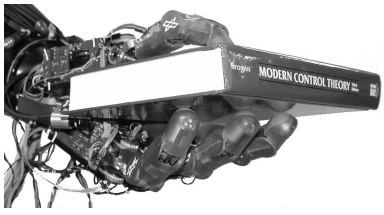


Figure 1. DLR Hand II grasping an object

This paper presents a way of estimating the position of contact and the normal of the contact surface, using

only joint position and velocity measurements, applying hand kinematics proposed in [22] and exploiting constraints on motion between finger and object when having a stable contact. This method additionally requires only a geometric description of the finger tips in contact, which usually is available. This method is valid for any type of contact providing enough constraints and any convex finger geometry. Section 2 of this paper revisits the kinematics of contact. From here the contact point is identified in section 3. An observer to track the contact point on the fly during manipulation is proposed in section 4. Results of simulation are presented in 5.

Throughout this paper, small bold letters represent vector and capital letters matrix quantities. The subscripts $w$, $o$ and $f$ mean world, object and finger related quantities, $fc$, and $oc$ mean contact on either finger or object side. An additional number or $i$ relates the quantity to the respective finger, whereas an additional $h$ means finger quantities stacked to a vector or matrix resulting in hand quantities.

## 2. Kinematics of Contact

In this chapter, a formula (c.f. eqn. 3) is derived, which relates the unknown object velocity to a measured finger velocity and an unknown relative velocity between finger and object. This equation is used in subsequent chapters to estimate the position of contact on the finger surface. The kinematics of one or multiple fingers grasping an object can best be described as presented in [22]. As shown in figure 2, the kinematic chain from a chosen world frame $S_w$ to an object frame $S_o$ consists, for each finger $i$ individually, of two partial chains. The first chain describes the position

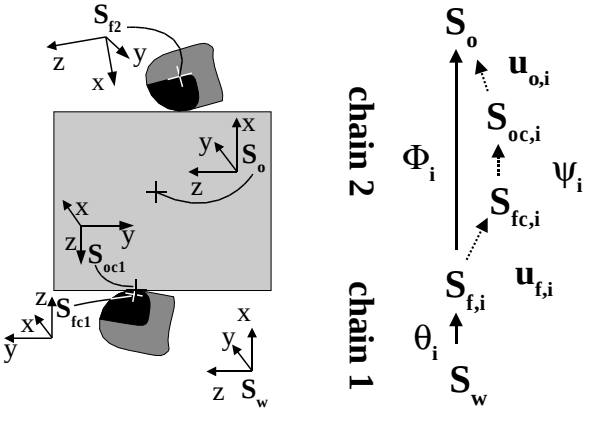


a) Coordinate Frames b) Kinematic Chains

Figure 2. Kinematics of Contact

and motion of a fixed point of the finger tip, the origin of $S_{f,i}$, e.g. the center of the tip's sphere. This chain can be formulated by the standard kinematic methods and depends only on the measurable joint angles $\boldsymbol{\theta}_i$. The second subchain relates the position of $S_{f,i}$ with that of the object $S_o$. This subchain itself may be considered as a series of three joints: One joint with two degrees of freedom, describing the position $\mathbf{u}_{f,i}$ of the contact point on the surface of the finger tip. A joint with one degree of freedom, describing the rotation $\psi$ between the two surfaces in contact. And another 2D joint describing the contact position $\mathbf{u}_{o,i}$ on the surface of the grasped object, c.f. figure 2 b). In the absence of image processing or tactile sensors the joint angles and velocities of the second subchain are not measurable directly.

Following the methodology of [22], the surface of finger tip $i$ and of the object are both represented as orthogonally parameterized functions $\Re^2 \rightarrow \Re^3$ : $\mathbf{f}_{f,i}(\mathbf{u}_{f,i})$ and $\mathbf{f}_o(\mathbf{u}_{o,i})$. The first is known, the latter is unknown and eliminated from the equations. The $x$– and $y$–axis of two coordinate systems $S_{fc,i}$ and $S_{oc,i}$ attached to the finger and the object side of the contact, c.f. figure 2 a), point into the direction of the partial derivative of the respective surface function $\mathbf{f}$ with respect to $u_1$ and $u_2$, the $z-$axis points outwards on the surface:

$$\begin{aligned} \mathbf{x}(\mathbf{u}) &= \frac{\partial \mathbf{f}}{\partial u_1} / \parallel \frac{\partial \mathbf{f}}{\partial u_1} \parallel, \\ \mathbf{y}(\mathbf{u}) &= \frac{\partial \mathbf{f}}{\partial u_2} / \parallel \frac{\partial \mathbf{f}}{\partial u_2} \parallel, \\ \mathbf{z}(\mathbf{u}) &= \mathbf{x}(\mathbf{u}) \times \mathbf{y}(\mathbf{u}) \end{aligned} \tag{1}$$

Equation (1) is valid for both sides of the contact, finger and object. Using (1), both 2D joints of chain 2 can be described as homogeneous transforms $\mathbf{T}_{f,i}^{fc,i}$ and $\mathbf{T}_{o}^{oc,i}$ from the contact systems $S_{fc,i}$ and $S_{oc,i}$ to systems $S_{f,i}$ and $S_o$, carrying the surfaces. The 1D joint relates both contact systems $S_{oc,i}$ and $S_{fc,i}$ to each other through $\mathbf{T}_{fc,i}^{oc,i}$:

$$\begin{aligned} \mathbf{T}_{f,i}^{fc,i} &= \begin{bmatrix} \mathbf{x}_{f,i}(\mathbf{u}_{f,i}) & \mathbf{y}_{f,i}(\mathbf{u}_{f,i}) & \mathbf{z}_{f,i}(\mathbf{u}_{f,i}) & \mathbf{f}_{f,i}(\mathbf{u}_{f,i}) \\ 0 & 0 & 0 & 1 \end{bmatrix} \\ \mathbf{T}_{o}^{oc,i} &= \begin{bmatrix} \mathbf{x}_{o,i}(\mathbf{u}_{o,i}) & \mathbf{y}_{o,i}(\mathbf{u}_{o,i}) & \mathbf{z}_{o,i}(\mathbf{u}_{o,i}) & \mathbf{f}_{o,i}(\mathbf{u}_{o,i}) \\ 0 & 0 & 0 & 1 \end{bmatrix} \\ \mathbf{T}_{fc}^{oc} &= \begin{bmatrix} \cos(\psi_i) & -\sin(\psi_i) & 0 & 0 \\ -\sin(\psi_i) & -\cos(\psi_i) & 0 & 0 \\ 0 & 0 & -1 & 0 \\ 0 & 0 & 0 & 1 \end{bmatrix} \end{aligned} \tag{2}$$

For each finger $i$, the generalized relative velocity $\mathbf{v}_o = [v_{o,x}, v_{o,y}, v_{o,z}, \omega_{o,x}, \omega_{o,y}, \omega_{o,z}]^T$ of $S_o$ with respect to $S_w$ can be expressed in coordinates of $S_w$ as sum of the velocity of the finger tip $\mathbf{v}_{f,i}$ in the first and the velocity along the contact $\mathbf{v}_{c,i}$ in the second subchain. Generally, $\mathbf{v}_{c,i}$ can be expressed in either of the contact systems. However, to relate $\mathbf{v}_{c,i}$ to a finger independent coordinate system $S_w$ or $S_o$, a combination of transforms of (2) has to be used, which all depend on the contact parameters $\mathbf{u}_{f,i}$, $\psi_i$ and $\mathbf{u}_{o,i}$. For

further computations, however, only $\mathbf{u}_{f,i}$ is of interest. Therefore, the system $S_{fc,i}$ was chosen as base for $\mathbf{v}_{c,i}$.

$$\begin{aligned} \mathbf{v}_o &= \mathbf{v}_{f,i} + \gamma_2^{-1}(\mathbf{T}_w^{f,i}(\boldsymbol{\theta}_i)\mathbf{T}_{f,i}^{fc,i}(\boldsymbol{\phi}_i))\mathbf{v}_{c,i} \\ &= \mathbf{J}_{f,i}(\boldsymbol{\theta}_i)\dot{\boldsymbol{\theta}}_i + \mathbf{J}_{c,i}(\boldsymbol{\theta}_i, \boldsymbol{\phi}_i)\mathbf{v}_{c,i} \qquad (3) \\ \text{with } \boldsymbol{\phi_i} &= [\mathbf{u}_{f,i}, \psi_i, \mathbf{u}_{o,i}]^T \\ \gamma_2^{-1} &: \begin{bmatrix} \mathbf{R} & \mathbf{d} \\ 0 & 1 \end{bmatrix} \rightarrow \begin{bmatrix} \mathbf{R} & (*\mathbf{d})\mathbf{R} \\ 0 & \mathbf{R} \end{bmatrix} \qquad (4) \\ * &: \begin{bmatrix} x \\ y \\ z \end{bmatrix} \rightarrow \begin{bmatrix} 0 & -z & y \\ z & 0 & -x \\ -y & x & 0 \end{bmatrix} \end{aligned}$$

where $\mathbf{J}_{f,i}$ and $\mathbf{T}_w^{f,i}$ are the finger Jacobian and the homogeneous transform from $S_w$ to $S_{f,i}$. The contact Jacobian $\mathbf{J}_{c,i}$ transforms velocities from the respective contact frame $S_{fc,i}$ to $S_w$. The vector $\boldsymbol{\phi}_i$ contains the contact joint parameters. The adjoint transformation $\gamma_2^{-1}(\mathbf{T}_A^B)$ performs a change of coordinates for velocities from system $B$ to system $A$ and the Hodge operator $*$ represents a vector cross product in matrix form as $*\mathbf{d}\ \mathbf{x} = \mathbf{d} \times \mathbf{x}$. Equation (3) describes the dependency of the object speed on the joint angles $\boldsymbol{\theta}_i$ and velocities $\dot{\boldsymbol{\theta}}_i$ on the one hand and the contact joint parameter $\boldsymbol{\phi}_i$ and the contact speed $\mathbf{v}_{c,i}$ on the other hand. The first two can be measured, the latter two are assumed unknown.

## 3. Contact point Identification

### 3.1. Interpretation of the Kinematics of Contact

In this section, from (3) a system of equations is derived in order to solve for the unknown $\boldsymbol{\phi}_i$ and $\mathbf{v}_{c,i}$. In $n$-fingered grasps, the unknown object speed $\mathbf{v}_o$ can be computed using any finger. Therefore it is possible to eliminate $\mathbf{v}_o$ by closing a loop over two fingers $i$ and $k$ along the way $S_w$, $S_{f,i}$, $S_o$, $S_{f,k}$ and back to $S_w$.

Choosing $n-1$ independent loops, a set of equations can be obtained:

$$\begin{aligned} 0 &= \mathbf{J}_{f,1}(\boldsymbol{\theta}_1)\dot{\boldsymbol{\theta}}_1 + \mathbf{J}_{c,1}(\boldsymbol{\theta}_1, \boldsymbol{\phi}_1)\mathbf{v}_{c,1} - \\ &\quad \mathbf{J}_{f,i}(\boldsymbol{\theta}_i)\dot{\boldsymbol{\theta}}_i - \mathbf{J}_{c,i}(\boldsymbol{\theta}_i, \boldsymbol{\phi}_i)\mathbf{v}_{c,i} \\ &\quad \text{with } 1 < i \leq n \qquad (5) \end{aligned}$$

Now, terms depending on the unknown contact joint parameters $\boldsymbol{\phi}_i$ and contact velocity $\mathbf{v}_{c,i}$ are brought on one side. Due to the choice of coordinates for $\mathbf{v}_{c,i}$ the contact Jacobian $\mathbf{J}_{c,i}$ depends only on $\mathbf{u}_{f,i}$ instead of the full $\boldsymbol{\phi}_i$. All $n-1$ equations are then stacked, forming the vector equation:

$$\mathbf{J}_{f,h}(\boldsymbol{\theta}_h)\dot{\boldsymbol{\theta}}_h = \mathbf{J}_{c,h}(\mathbf{u}_{f,h})\mathbf{v}_{c,h} \qquad (6)$$

where $\mathbf{v}_{c,h} = [v_{c,1}, ...v_{c,n}]^T$, $\boldsymbol{\theta}_h$, $\dot{\boldsymbol{\theta}}_h$ and $\mathbf{u}_{f,h}$ are defined analogously. The measurement vector $\Delta\mathbf{v}_{f,h} = \mathbf{J}_{f,h}(\boldsymbol{\theta}_h)\dot{\boldsymbol{\theta}}_h$ represents the relative finger velocity, $\mathbf{J}_{f,h}$ and $\mathbf{J}_{c,h}$ are block matrices containing the respective matrices of each finger stacked in a way as depicted in figure 3 for the three finger case. In the $n$ finger case,

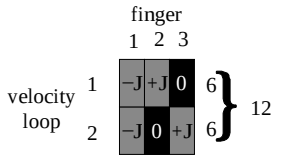


Figure 3. Structure of $\mathbf{J}_{c,h}$ and $-\mathbf{J}_{f,h}$

(6) represents a set of $6(n-1)$ equations with $6n$ unknown contact velocities $\mathbf{v}_{c,h}$ and $2n$ unknown contact joint parameters $\mathbf{u}_{f,h}$. However, the fingers grasping the object obey certain conditions in order to keep contact. These conditions describe the type of contact and can best be formulated in terms of the contact velocities $\mathbf{v}_{c,i}$ of each finger. A sliding contact is characterized by $v_{z,i} = \omega_{x,i} = \omega_{y,i} = \omega_{z,i} = 0$, plain rolling by $v_{x,i} = v_{y,i} = v_{z,i} = \omega_{z,i} = 0$ and rolling with twist by $v_{x,i} = v_{y,i} = v_{z,i} = 0$. The $l$ contact conditions render $nl$ additional equations, in the plain rolling case $4n$ and in the case allowing twist $3n$. Incorporating these contact conditions into (6), $\mathbf{v}_{c,h}$ is reduced to its non–zero components $\tilde{\mathbf{v}}_{c,h}$ and $\mathbf{J}_{c,h}$ is adjusted appropriately as $\tilde{\mathbf{J}}_{c,h}$. In order to compute the contact joint parameters $\mathbf{u}_{f,i}$ and therefore the contact point of each finger with the object and direction of the surface normal, (6) has to be solved for $\tilde{\mathbf{v}}_{c,h}$ and $\mathbf{u}_{f,h}$. The adjusted system of (6) then represents a set of $6(n-1)$ equations in $(6-l)n+2n$ unknowns. Considering that, when performing small finger movements or returning to the starting position after a test motion, the contact joint parameters $\mathbf{u}_{f,h}$ behave like state variables and vary only little, it is possible to increase the number of equations by repetitively moving the fingers locally around a test configuration in different directions and sampling $\Delta\mathbf{v}_{f,h}$. The dependency between the $\Delta\mathbf{v}_{f,h}$ and $\tilde{\mathbf{v}}_{c,h}$ is linear, whereas $\mathbf{u}_{f,h}$ has a nonlinear dependency. This suggests that, for the solvability of (6), there exist three different cases:

- First, the system is completely solvable or overdetermined in all, linearly and nonlinearly dependent unknowns.

- Second, the system is overdetermined in the rapidly varying linearly dependent $\tilde{\mathbf{v}}_{c,h}$, however underdetermined in general, thus several samples have to be evaluated.

- Third, even with an arbitrarily large number of samples, the system remains underdetermined.

The three cases are summarized in table 1 along with examples for a 3-fingered setup and a scenario of rolling with twist, which in the sequel is the example setup. As can be seen from this table, in common dextrous manipulation setups neither case 1 nor case 3 can usually be achieved. The first is irrelevant due

| case | condition | description | $n=3$ | $l=3$ |
|---|---|---|---|---|
| 1 | $l\ n \geq 6+2n$ | generally (over-) determined | $l \geq 4$ | $n \geq 6$ |
| 2 | $6 < l\ n < 6+2n$ | overdetermined in $\hat{\mathbf{v}}_c$ | $2 < l < 4$ | $2 < n < 6$ |
| 3 | $6 \geq l\ n$ | generally underdetermined | $l \leq 2$ | $n \leq 2$ |

Table 1. Solvability of Contact Equation

to the large number of fingers and contact constraints, the second due to the small number of fingers and motion constraints. The most common case 2 is therefore investigated here.

### 3.2. Formulation as Optimization Problem

Considering case 2 of table 1, it is possible to interprete (6) as a mapping $\Gamma$ from the space $\mathcal{C} = \Re^{(6-l)n}$ of reduced contact velocities $\tilde{\mathbf{v}}_{c,h}$ to the space $\mathcal{F} = \Re^{6(n-1)}$ of relative finger velocities $\Delta\mathbf{v}_{f,h}$, where $\dim(\mathcal{F}) > \dim(\mathcal{C})$. Thus, the mapping $\Gamma$ has a left nullspace $\mathcal{L}$ which is the orthogonal complement of $\text{range}(\Gamma) = \text{range}(\tilde{\mathbf{J}}_{c,h})$ in $\mathcal{F}$. In a strict sense, $\Delta\mathbf{v}_{f,h}$ and $\tilde{\mathbf{v}}_{c,h}$ contain values with different units rendering a scalar product impossible. In the sequel these values are considered weighted by an appropriate factor. In formulas given, this weighting is omited for clarity. One possible map $\Gamma^{-1}$ from $\mathcal{F}$ to $\mathcal{C}$ is the left pseudoinverse $\tilde{\mathbf{J}}^{+}_{c,h}$, which returns in the sense of least squares the best possible estimate $\hat{\mathbf{v}}_{c,h}$ for a measured $\Delta\mathbf{v}^{*}_{f,h}$. Both mappings are shown in figure 4. They depend on the unknown contact joint parameters $\mathbf{u}_{f,h}$. As can be

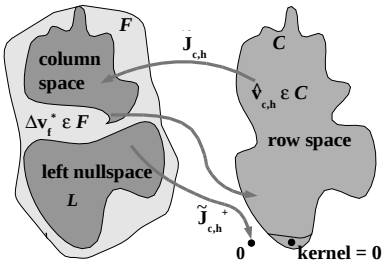


Figure 4. Mappings of the Contact Jacobian

seen from figure 4, the relative velocity $\Delta\mathbf{v}^{*}_{f,h}$ has usually components from either of the two subspace of $\mathcal{F}$. When mapping $\Delta\mathbf{v}^{*}_{f,h}$ to $\mathcal{C}$, its components parallel to $\mathcal{L}$ are projected to $\mathbf{0}$. These are the components that cause an error to occur in the least squares fit of $\tilde{\mathbf{J}}^{+}_{c,h}$. The components of $\Delta\mathbf{v}^{*}_{f,h}$ orthogonal to $\mathcal{L}$ are mapped to its unique image $\hat{\mathbf{v}}_{c,h}$ in $\mathcal{C}$. Projecting $\hat{\mathbf{v}}_{c,h}$ back to $\mathcal{F}$ results in the original components of $\Delta\mathbf{v}^{*}_{f,h}$ orthogonal to $\mathcal{L}$. With this result the components of $\Delta\mathbf{v}^{*}_{f,h}$ parallel to $\mathcal{L}$ can be computed:

$$\mathbf{e}_{f,h} = \Delta\mathbf{v}^{*}_{f,h} - \tilde{\mathbf{J}}_{c,h}\tilde{\mathbf{J}}^{+}_{c,h}\Delta\mathbf{v}^{*}_{f,h} \tag{7}$$

In a consistent setup, the mapping $\Gamma^{-1}$ is bijective for the space of actual measurements $\Delta\mathbf{v}^{*}_{f,h}$, which then lie in the range of $\tilde{\mathbf{J}}_{c,h}$, and therefore $\mathbf{e}_{f,h} = \mathbf{0}$. Taking any norm of $\mathbf{e}_{f,h}$ renders a measure $L$ for this inconsistency of the mapping $\Gamma^{-1}$. Since the mappings $\Gamma$ and $\Gamma^{-1}$ depend on the contact joint parameters $\mathbf{u}_{f,h}$, so does $\mathbf{e}_{f,h}$ and consequently $L$:

$$L(\mathbf{u}_{f,h}, \Delta\mathbf{v}^{*}_{f,h}) = \mathbf{e}^{T}_{f,h}(\mathbf{u}_{f,h})\mathbf{e}_{f,h}(\mathbf{u}_{f,h}) \tag{8}$$

With $m$ different measurements of $\Delta\mathbf{v}^{*}_{f,h}$, it is possible to solve not only for $\hat{\mathbf{v}}_{c,h}$ but also get a better estimate $\hat{\mathbf{u}}_{f,h}$ for $\mathbf{u}_{f,h}$ by minimizing $L$ over $\mathbf{u}_{f,h}$:

$$\hat{\mathbf{u}}_{f,h} : L(\hat{\mathbf{u}}_{f,h}) = \min_{\mathbf{u}_{f,h}} \sum_{i=1}^{m} L(\mathbf{u}_{f,h}, \Delta\mathbf{v}^{*}_{f,h,i}) \tag{9}$$

As shown above, several measurements are always required. One single measurement only causes significant errors $L$ along a particular direction of $\mathbf{u}_{f,i}$, whereas in other directions $L$ varies only little. From here, with estimates of the contact parameter $\hat{\mathbf{u}}_{f,i}$ and the contact velocity $\hat{\mathbf{v}}_{c,i}$, the desired exteroceptive information, the position of the contactpoint $\mathbf{r}_{c,i}$, the normal direction on the contact surface $\mathbf{n}_{c,i}$ and the object velocity $\mathbf{v}_o$ can be computed:

$$\begin{aligned} \mathbf{r}_{c,i} &= \mathbf{T}^{f,i}_{w}(\theta_i)\mathbf{f}_{f,i}(\hat{\mathbf{u}_{f,i}}) \\ \mathbf{n}_{c,i} &= \mathbf{T}^{f,i}_{w}(\theta_i)\mathbf{T}^{fc,i}_{f,i}(\hat{\mathbf{u}}_{f,i})\,[0,0,1,0]^{T} \\ \mathbf{v}_o &= \mathbf{J}_{f,i}(\boldsymbol{\theta}_i)\dot{\boldsymbol{\theta}}_i + \mathbf{J}_{c,i}(\boldsymbol{\theta}_i, \boldsymbol{\phi}_i)\hat{\mathbf{v}}_{c,i} \end{aligned} \tag{10}$$

## 4. Observer Based Correction

On individual or multiple measurements with the actual contact parameters not varying, section 3.2 provides a measure of how inaccurate an estimate $\hat{\mathbf{u}}_{f,h}$ of the contact joint parameters is. However, in the presence of measurement disturbances or a violation of the condition of a nearly constant $\mathbf{u}_{f,h}$ an observer will render better results for $\hat{\mathbf{u}}_{f,h}$. An observer concept dual to Kalman-filtering is proposed, as shown in figure 5. This, in a first step, minimizes a given $\chi$-function. This function first puts a penalty on the mismatch between the measurement $\Delta\mathbf{v}^{*}_{f,h}$ and the estimate $\mathbf{J}_{c,h}\hat{\mathbf{v}}_{c,h}$, c.f. (6), and second on a mismatch between a previous estimate $\hat{\mathbf{u}}_{f,h}(t)$ and the recent estimate $\bar{\mathbf{u}}_{f,h}(t)$. The contact velocity is also compared to it's previous value to suppress unlikely large changes but is weighted little. From here we get an estimate for $\mathbf{v}_{c,h}(t)$ and an improvement of the previous estimate

of $\hat{\mathbf{u}}_{f,h}(t)$. To perform the minimization a Levenberg-Marquard algorithm is used. In a second, dynamic step, the improved estimate $\bar{\mathbf{u}}_{f,h}(t)$ is propagated to time $t+1$ using kinematics from [21]. The unknown surface parameters of the object are approximated as a plane. This is reasonable for common objects with a curvature not too large.

Levenberg-Marquard step:

$$\chi(\mathbf{u}_{f,h}, \mathbf{v}_{c,h}) =$$
$$\frac{1}{2}\left(\Delta\mathbf{v}^*_{f,h}(t) - \tilde{\mathbf{J}}_{c,h}(\mathbf{u}_{f,h})\mathbf{v}_{c,h}\right)^T$$
$$\mathbf{C}_m^{-1}\left(\Delta\mathbf{v}^*_{f,h}(t) - \tilde{\mathbf{J}}_{c,h}(\mathbf{u}_{f,h})\mathbf{v}_{c,h}\right)$$
$$+\frac{1}{2}\left([\mathbf{v}_{c,h}(t), \mathbf{u}_{f,h}(t)]^T - [\hat{\mathbf{v}}_{c,h}(t-1), \hat{\mathbf{u}}_{f,h}(t)]^T\right)^T$$
$$\mathbf{C}_s^{-1}(t)\left([\mathbf{v}_{c,h}(t), \mathbf{u}_{f,h}(t)]^T - [\hat{\mathbf{v}}_{c,h}(t-1), \hat{\mathbf{u}}_{f,h}(t)]^T\right)$$
$$[\hat{\mathbf{v}}_{c,h}(t), \bar{\mathbf{u}}_{f,h}(t)] : \min_{\hat{\mathbf{v}}_{c,h}(t), \bar{\mathbf{u}}_{f,h}(t)} \chi(\hat{\mathbf{v}}_{c,h}(t), \bar{\mathbf{u}}_{f,h}(t))$$

Dynamic step for each finger:

$$\hat{\mathbf{u}}_{f,i}(t+1) = \mathbf{M}_{f,i}^{-1}\mathbf{K}_f, i^{-1}\mathbf{S}\hat{\mathbf{v}}_{c,i}\Delta t + \bar{\mathbf{u}}_{f,i}(t)^0$$
$$\mathbf{S} = \begin{bmatrix} 0 & 0 & 0 & 0 & -1 & 0 \\ 0 & 0 & 0 & 1 & 0 & 0 \end{bmatrix}$$
$$\mathbf{C}_s(t+1) = \frac{d^2\chi}{d\left([\hat{\mathbf{v}}_{c,h}(t), \hat{\mathbf{u}}_{f,h}(t)]^T\right)^2} + \mathbf{C}_z \quad (11)$$

where $\mathbf{C}_m$, $\mathbf{C}_s$ and $\mathbf{C}_z$ are the measurement, the system and the state covariance matrix respectively, $\mathbf{S}$ is a selection matrix, $\mathbf{M}_{f,i}$ and $\mathbf{K}_f, i$ are the metric and curvature matrix of the finger as defined in [21].

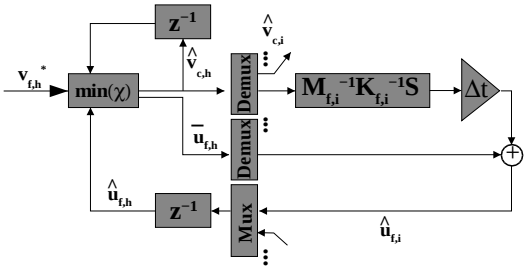


Figure 5. Structure of Observer

## 5. Results of Simulations

The algorithms previously presented have been tested using a kinematic simulation of the 4-finger DLR Hand II, neglecting the ring finger for simplicity. The finger tips have been modeled as spheres using a parameterization in sphere coordinates with the longitude $u_{f1,i} = 0$ centered on the palm side of each finger $i$ and the latitude $u_{f2,i} = 0$ being at the north pole of the sphere. The contact allows rolling with twist and has thus all 3 rotational degrees of freedom, restricting translations. A grasp as shown in figure 6 has been

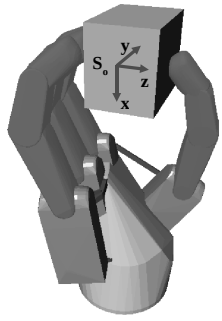


Figure 6. DLR-Hand grasping an Object

performed with the contact joint parameters being located at $[0, 60°, 0, 30°, 0, 30°]^T$. First, to illustrate the nature of the error landscape produced by (8), the error function was evaluated for different estimates of the contact parameters. Hereby the grasped object was moved in either of the three rotational degrees of freedom. For evaluation, an optimized algorithm similar to Gram-Schmidt orthogonalization was used, wich needed about 1 ms for each point to be computed. For reduction to a two dimensional landscape, the longitudinal parameter estimates $\hat{u}_{f1,i}$ were kept at their real values $u_{f1,i}$, and the latitudes of fingers 2 and 3 $\hat{u}_{f2,i}$ were kept identical. The results have been depicted as density plots with $L$ being evaluated logarithmically due to large changes in magnitude in figure 7. As can be seen, for all motions the landscape is valley like, with one direction being rather flat and the minimum of $L$ being at the true value of $\mathbf{u}_{f,h}$. Those motions of the object (a,b) causing rolling of the fingers across latitude lines, result in a distinct valley in the chosen 2D error landscape, which is more distinct in (b) because here the motions orthogonally cross latitudes, whereas in (a) a crossing of latitudes is under a smaller angle. Other motions (c), causing twist, do exhibit only a small dip. In the flat direction, evaluation of $L$ obviously returned only little information. However, depending on the object velocity, the direction of the valley changes. Thus an observer can find the intersection of all these valleys when suitable object motions are performed.

Now, the performance of the observer was examined under different object velocities. The simulation was run on a SGI Onyx II with R10K 195 MHz processor. For the minimization a Levenberg-Marquard algorithm was used which relies on SVD of dimension 15 for equation solving and an inversion of 12 for computation of time variant $C_m^{-1}$, in the dynamic step two matrix inversions of dimension 15 and 6 respectively are necessary for update of $C_s^{-1}$. After the first run the

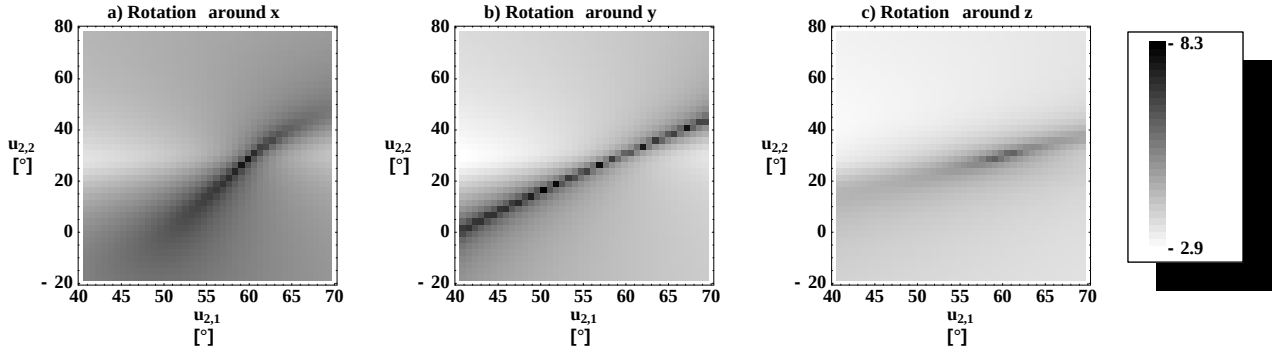


Figure 7. Error Landscape with Different Object Velocities

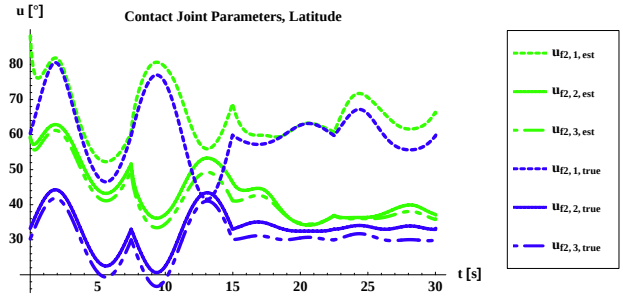


Figure 8. Observation of the latitudinal contact parameter $\mathbf{u}_{f2,i}$ for 30 s with 25 ms sampling time and varying object velocities

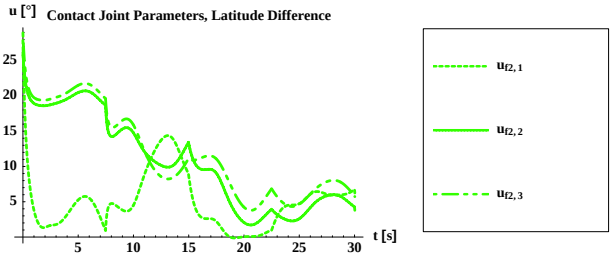


Figure 9. Error between estimated and true contact parameter

number of iterations in the L/M algorithm settles at 1. The average execution time for a whole cycle of the observer then was around 5 ms. The grasped object was moved in space for a total duration of $30s$ with several sinusoidal velocities of a frequency of $1/7.5Hz$ for $7.5s$ each. The different translational and angular velocities varied in amplitude and direction. In the simulation, the sampling rate was $25ms$. For a better visibility in the plots, here $u_{f2,2}$ started at 33°. In figure 8, the true $\mathbf{u}_{f,h}$ and the estimated $\hat{\mathbf{u}}_{f,h}$ latitudinal contact parameters are depicted over time as dark and bright lines respectively. One can observe that, while following the general motion of the true values, the estimates converge to a neighborhood of about $5° - 7°$ to its real value. Some motions can be tracked better than others, thus convergence rate changes with different $\mathbf{v}_o$. This was predicted in section 3.2. The difference between true and estimated contact parameters is depicted in figure 9. It can be seen that, during some object motions, no information about the contact point error can be obtained. Thus the evolution of $\hat{\mathbf{u}}_{f,h}$ completely relies on extrapolation and the difference between true and estimated values increases again. The remaining error in the longitudinal direction settles at about 20°. This translates to an estimation which lies in an area of only $2mm^2$ around the true position due to the spherical coordinate system.

## 6. Conclusions

In this paper, based on the kinematics of contact, a method has been proposed, to determine the error in an estimate of the contact joint parameters. With these estimates, the position of the contact point between finger and object on the fingersurface and the normal direction on the object surface can be computed. Second, an observer structure dual to a Kalman filter has been proposed, which allows computation of these exteroceptive information on the fly during grasping and thus observe the rolling motion of the fingers on the object. This information can for example be applied to methods used for synthesizing grasps, grasp control and grasp force optimization. The validity of the taken approach has been verified in simulations. Further work has to be done, examining the

observer with respect to sensitivity to noise, developing optimal object motions for detection, applying the proposed algorithms to an experimental setup and examine the applicability for enhanced object controllers used for manipulation.

## References


[1] A. Bicchi and V. Kumar. Robotic grasping and contact: A review. In *Proceedings of the IEEE International Conference on Robotics and Automation April 2000, San Francisco, California*, pages 348 – 353, 2000.

[2] A. Bicchi, A. Marigo, and D. Prattichizzo. Dexterity through rolling: Manipulation of unknown objects. In *Proceedings of the IEEE International Conference on Robotics and Automation May 1999, Detroit, Michigan*, pages 1583 – 1588, 1999.

[3] A. Bicchi, J. K. Salisbury, and D. L. Brock. Contact sensing from force measurements. *International Journal of Robotics Research*, 12(3), 1993.

[4] C. Borst, M. Fischer, and G. Hirzinger. A fast and robust grasp planner for arbitrary 3d objects. In *Proceedings of the IEEE International Conference on Robotics and Automation May 1999, Detroit, Michigan*, pages 1890–1896, 1999.

[5] M. Buss and T. Schlegl. Multi-fingered regrasping using on-line grasping force optimization. In *Proceedings of the IEEE International Conference on Robotics and Automation, April 1997, Albuquerque, New Mexico*, pages 998 – 1003, 1997.

[6] J. Butterfaß, M. Grebenstein, H. Liu, and G. Hirzinger. DLR-hand II: Next generation of a dextrous robot hand. In *Proceedings of the IEEE International Conference on Robotics and Automation May 2001, Seoul ,Korea*, 2001.

[7] J. Butterfaß, S. Knoch, H. Liu, and G. Hirzinger. DLR's multisensory articulated hand part I: Hard- and software architecture. In *Proceedings of the IEEE International Conference on Robotics and Automation May 1998, Leuven, Belgium*, pages 2081 – 2086, 1998.

[8] S. Caselli, C. Magnanini, F. Zanichelli, and E. Caraffi. Efficient exploration and recognition of convex objects based on haptic perception. In *Proceedings of the IEEE International Conference on Robotics and Automation, April 1996, Minneapolis, Minnesota*, 1996.

[9] M. Charlebois, K. Gupta, and S.Payandeh. Shape description of curved sufaces from contact sensing using surface normals. *International Journal of Robotics Research*, 18(8):779–787, August 1999.

[10] R. S. Fearing. Tactile sensing for shape interpretation. In S. Venkataraman and T. Iberall, editors, *Dextrous Robot Manipulation*, chapter 10. Springer-Verlag, 1990.

[11] R. A. Grupen and M. Huber. 2-d contact detection and localization using proprioceptive information. In *Proceedings of the IEEE International Conference on Robotics and Automation 1993*, 1993.

[12] S. Haidacher, T. Schlegl, and M. Buss. Grasp evaluation based on unilateral force closure. In *Proceedings of the IEEE/RSJ Intl. Conference on Intelligent Robots and Systems 1999, Kyongju, Korea*, pages 424 –429, 1999.

[13] L. Han, J. C. Trinkle, and Z. Li. Grasp analysis as linear matrix inequality problems. In *Proceedings of the IEEE International Conference on Robotics and Automation May 1999, Detroit, Michigan*, pages 1261 – 1268, 1999.

[14] Y. B. Jia and M. Erdmann. Pose and motion from contact. *International Journal of Robotics Research*, 18(5):466 – 490, May 1999.

[15] M. Kaneko and K. Tanie. Contact point detection for grasping of an unknown object using self-posture changeability (spc). In *Proceedings of the IEEE International Conference on Robotics and Automation 1990*, 1990.

[16] R. L. Klatzky and S. Lederman. Intelligent exploration by the human hand. In S. Venkataraman and T. Iberall, editors, *Dextrous Robot Manipulation*, chapter 4. Springer-Verlag, 1990.

[17] H. Liu and G. Hirzinger. Cartesian impedance control for the DLR hand. In *Proceedings of the IEEE/RSJ Intl. Conference on Intelligent Robots and Systems 1999, Kyongju, Korea*, pages 106 – 112, 1999.

[18] H. Maekawa, K. Tanie, and K. Komoriya. Tactile sensor based manipulation of an unknown object by a multifingered hand with rolling contact. In *Proceedings of the IEEE International Conference on Robotics and Automation, May 1995, Nagoya, Japan*, 1995.

[19] M. T. Mason and J. K. Salisbury. *Robot Hands and the Mechanics of Manipulation*. The MIT Press, Cambridge, MA, 2 edition, 1986.

[20] N. Mimura and Y. Funahashi. Parameter identification in the grasp of an inner link mechanism. In *Proceedings of the IEEE International Conference on Robotics and Automation 1993*, 1993.

[21] D. J. Montana. The kinematics of contact and grasp. *International Journal of Robotics Research*, 7(3):17 – 32, June 1988.

[22] D. J. Montana. The kinematics of multi-fingered manipulation. *IEEE Transactions on Robotics and Automation*, 11(4):491 – 503, August 1995.

[23] A. M. Okamura and M. R. Cutkosky. Haptic exploration of fine surface features. In *Proceedings of the IEEE International Conference on Robotics and Automation May 1999, Detroit, Michigan*, 1999.

[24] T. Schlegl, S. Haidacher, M. Buss, F. Freyberger, F. Pfeiffer, and G. Schmidt. Compensation of discrete contact state errors in regrasping experiments with the TUM-hand. In *Proceedings of the IEEE/RSJ Intl. Conference on Intelligent Robots and Systems 1999, Kyongju, Korea*, pages 118 – 123, 1999.